Cellulose (2022) 29:4413–4426
https://doi.org/10.1007/s10570-022-04511-y

ORIGINAL RESEARCH

Preparation and properties of epichlorohydrin-cross-linked chitosan/hydroxyethyl cellulose based CuO nanocomposite films

Xueqin Zhang · Haoqi Guo · Naiyu Xiao · Xinye Ma · Chuanfu Liu · Le Zhong · Gengsheng Xiao

Received: 17 August 2021 / Accepted: 28 February 2022 / Published online: 6 April 2022

Abstract This study introduces an effective route to fabricate chitosan (CS)-based film. The films were prepared through cross-linking reaction between CS and hydroxyethyl cellulose (HEC) using epichlorohydrin (ECH) as the cross-linker and simultaneously in-situ loading with CuO nanoparticles. FT-IR and loading efficiency results indicated the occurrence of inter- and intra-molecular cross-linking reaction between CS and HEC. XRD and EDS analyses showed that the CuO nanoparticles were evenly deposited onto CS film matrixes. SEM characterization showed that the films were of compact, dense and uniform cross morphologies, as well as obvious voids. The films also exhibited desired swelling ratio and water vapor permeability. The enhanced tensile strength was obtained with a maximum value of 77.02 ± 3.26 MPa, while the stretch-ability slightly decreased. The thermal stability of the films decreased after cross-linking with HEC. The antibacterial ability of the films was generally improved with the increase of HEC and ECH contents.

X. Zhang · H. Guo · N. Xiao (✉) · L. Zhong · G. Xiao (✉)
College of Light Industry and Food Technology, Zhongkai University of Agriculture and Engineering, Guangzhou 510225, China
e-mail: xiaony@163.com

G. Xiao
e-mail: Gshxiao@aliyun.com

X. Zhang · N. Xiao · L. Zhong · G. Xiao
Academy of Contemporary Agricultural Engineering Innovations, Zhongkai University of Agriculture and Engineering, Guangzhou 510225, China

X. Zhang · N. Xiao · L. Zhong · G. Xiao
Guangdong Key Laboratory of Science and Technology of Lingnan Specialty Food, Zhongkai University of Agriculture and Engineering, Guangzhou 510225, China

X. Zhang · C. Liu (✉)
State Key Laboratory of Pulp and Paper Engineering, South China University of Technology, Guangzhou 510640, China
e-mail: chfliu@scut.edu.cn

X. Ma
Key Laboratory of Chinese Medicinal Resource From Lingnan, Ministry of Education, Guangzhou University of Chinese Medicine, Guangzhou 510006, China

Graphical abstract Preparation and properties of epichlorohydrin-cross-linked chitosan/hydroxyethyl cellulose based CuO nanocomposite films

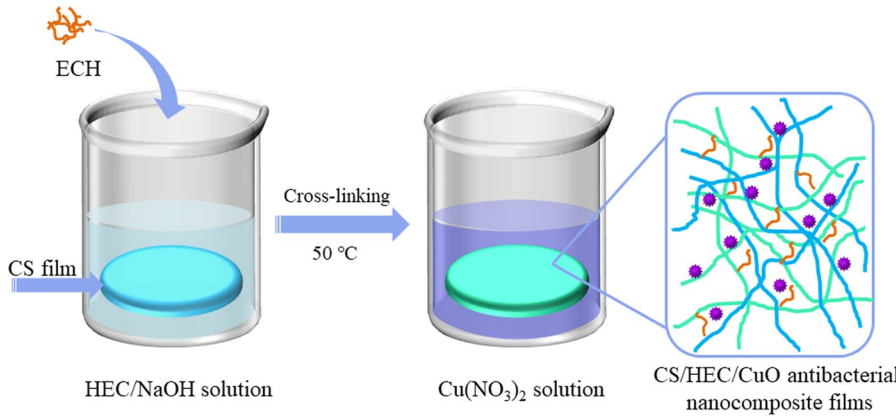

Keywords Chitosan · Hydroxyethyl cellulose · Cross-linking · Nanocomposite films · Functional properties

Introduction

Microorganism contamination is still a major threat to food safety that may cause enormous socio-economic and health problems. Normally, plastic films combining with chemical antibiotics are the primary preservative methods to guarantee food qualities. However, packaging films produced from conventional synthetic petroleum based polymers are non-biodegradable. And the overuse of chemical antibiotics will result in the emergence of drug-resistant pathogens (Guo et al. 2015; Joubert et al. 2015). This makes a way for the application of biodegradable polymers in packaging area (Ebrahimi et al. 2019; Xie et al. 2020). An ideal packaging film should be of high efficiency, good antibacterial ability, low cost, and easy synthesis. Therefore, renewable resources such as cellulose (Wang et al. 2019), chitosan (CS) (Min et al. 2020; Zhang et al. 2019a), hemicelluloses (Arellano-Sandoval et al. 2020; Yousefi et al. 2020) and starch (Wang et al. 2021; Yuan et al. 2020) have attracted great attention.

CS is obtained from chitin, a biopolymer which can be extracted from crustacea, fungi and insects (Kumar et al. 2019). Because of the good film-forming ability and natural antibacterial activity, CS has been extensively applied in food, pharmacy, medical treatment, and packaging areas (Siripatrawan and Kaewklin 2018; Yu et al. 2018). However, pure CS film is not satisfactory for packaging because of its limited antibacterial ability and flexibility (Verlee et al. 2017). In terms of these, blending with other polymers, using cross-linkers, and incorporation of micro or nanofiller into CS matrixes are some of the effective ways that have been used to improve the properties of CS films. Among these methods, developing nanocomposites with good antibacterial activity have been studied extensively.

CS contains primary amino and primary alcohol on the D-glucosamine unit. The different reactivities of these functional groups make CS can be easily self-cross-linked or cross-linked with other polymers, therefore improving the transparency, mechanical strength, and homogenous surfaces of CS film. Tannic acid, glutaraldehyde, and epichlorohydrin (ECH) are frequently used as chemical cross-linkers for film fabrication. ECH is a cross-linking agent of polymers by forming a glycidylether linkage through the reactions between hydroxyl groups on polysaccharide. The films based on ECH cross-linked CS showed promising mechanical properties. For example, Guan et al. (Guan et al. 2016) prepared drug-loading film by the cross-linking reaction of quaternized hemicelluloses and CS using ECH as the cross-linker, and the resulting film exhibited an excellent mechanical performance with tensile strength up to 37 MPa; Yeng

et al. (Yeng et al. 2015) developed CS and corn cob bio-composite films by cross-linking with ECH, and the highest tensile strength and elongation at break of the film were 46.9 ± 0.9 MPa and 8.2 ± 0.4%, respectively; Cao et al. (Cao et al. 2018) fabricated ECH cross-linked CS films, and found a significant increase in mechanical properties compared with non-cross-linked CS films (Cao et al. 2012). From this point, it would be of great interest for further improving the mechanical properties of CS films by cross-linking method.

Also, in this study, antibacterial ability of CS film is the other target property that needs to be developed. Metal oxide nanostructures exhibited great potential in the area of developing new functional materials and nanomaterials due to their unique chemical and physical properties (Ebrahimi et al. 2019; Raghavendra et al. 2017; Xie et al. 2020; Zhang et al. 2020). Recently, copper oxide nanoparticles (CuO) have received great attention, mainly considering its special electrical, optical as well as antimicrobial properties, which show broad applications in gas sensors, lithium battery, heterogeneous catalysts, and antimicrobial materials (Čech Barabaszová et al. 2020). The formation of antimicrobial properties of copper nanoparticles is due to its ability to capture electrons, so it possesses great catalytic activity for oxidation and reduction reactions (Ebrahimi et al. 2019). CuO can interference with nucleic acids, and the active site of enzymes and cell wall components, causing the death of microbial cells (Ebrahimi et al. 2019; Peighambardoust et al. 2016). Nevertheless, direct mechanical mixing of CuO in polymer film can obtain microscale interaction between CuO and matrix, leading to poor mechanical properties and dispersibility (Fu et al. 2015). Using chemical methods, like precipitation and sol–gel approaches, to synthesize CuO nanoparticles have shown some distinct advantages over mechanical mixing and physical methods, including feasible size control of CuO nanoparticles and inexpensive equipment required (Almasi et al. 2019; Booshehri et al. 2015). These processes were normally conducted in an alkaline or alcohol solution, and copper salts like $CuCl_2$, $Cu(CH_3COO)_2$, $CuSO_4$, and $Cu(NO_3)_2$ were used as the precursors (Almasi et al. 2019; Booshehri et al. 2015). Traditionally, CS was used as a growth medium of CuO due to its restricted solubility in acidic solution. In one instance, Raghavendra et al. (Raghavendra et al. 2017) reported CuO nanoparticles with flower-like morphology, which were synthesized using CS as a growth medium in an ammonia solution. However, only a few studies have been reported concerning the fabrication of CS-based antibacterial films with in-situ grown CuO nanoparticles.

The objective of this study was to prepare a new antibacterial CS nanocomposite film with good mechanical properties. In terms of this, we developed an effective method of simultaneous cross-linking and in-situ loading. Specifically, ECH mediated cross-linking reaction between CS and HEC was carried out in NaOH solvent, and in-situ loading of CuO onto CS matrix was occurred at the same time. The morphology, structure, and physicochemical properties of the films were comprehensively investigated.

Experimental

Materials

CS (medium viscosity, 200–400 mPa.s), HEC (1500–2500 mPa.s), ECH (99.5%, GC), $Cu(NO_3)_2{\cdot}3H_2O$ (99.99% metals basis) were purchased from Shanghai Macklin Biochemical Co., Ltd. (Shanghai, China). All other reagents were of analytical grade and commercially available.

Preparation of the cross-linked CS nanocomposite films

CS (1 g) was dissolved in 20 mL 0.1 M glacial acetic acid and dried to obtain the films. Then the CS films were soaked in 0.25 M NaOH aqueous solution with HEC of 0.2:1, 0.4:1, 0.6:1, 0.8:1 and 1:1 (relative to CS, w/w) and ECH of 5%, 10%, 15%, 20% and 25% (relative to CS, v/w), and cross-linked at 50 °C for 4 h. After that, the cross-linked films were soaked in 0.5 M $Cu(NO_3)_2{\cdot}3H_2O$ solution at room temperature overnight before washed with deionized water till neutral and dried. The obtained films were designated as CSxHyE, where x and y denoted the contents of HEC and ECH, respectively. HEC loading efficiency (L) of the films was studied by gravimetric method according to the following equation. Each experiment was repeated for three times.

$$L(\%) = \frac{W_l - W_i}{W_i} \times 100\% \quad (1)$$

where W_i and W_l are the weights of the films before and after cross-linking with HEC, respectively.

Pure CS film reinforced with CuO nanoparticles was prepared without cross-linking with HEC. To synthesize CuO nanoparticles, a reported method was used (Booshehri et al. 2015). Briefly, 20 mL of 0.25 M NaOH aqueous solution was poured into 5 mL 0.5 M $Cu(NO_3)_2{\cdot}3H_2O$ solution, and the mixture was continuously stirred overnight at room temperature. The obtained solids were washed with deionized water till neutral and dried at 60 °C.

Characterization

Fourier transform infrared spectroscopy (FT-IR) was carried out on Vetex 70 spectrometer (Bruker, Germany) using attenuated total reflectance accessory over a range of 4000–500 cm^{-1} at a resolution of 4 cm^{-1}.

Scanning electron microscopy (SEM) was conducted on a LEO 1530 VP equipment (Germany) at 10 kV.

Transmission electron microscopy (TEM) of CuO nanoparticles was characterized by FEI Tecnai G2 f20 s-twin at 200 kv with point resolution of 0.24 nm. Before measurements, CuO nanoparticles were evenly dispersed in ethanol.

Elemental mapping and energy dispersive X-ray spectroscopy (EDS) data were collected using Zeiss Sigma 300.

Thermal stability (TGA/DTG) was carried out on TGA500 simultaneous thermal analyzer (TA, USA). The measurement was performed at a heating rate of 15 °C/min over a temperature range of 30–700 °C. Nitrogen gas was applied as the purge gas at a flow rate of 25 mL/min.

X-ray diffraction (XRD) was conducted on a D/max-III X-ray diffractometer (Japan) equipped with nickel filtered Cu Kα radiation in the diffraction angle ranges of 5–80°.

Equilibrium-swelling ratio (*SR*, %) of the films was determined according to the previously reported method (Yao et al. 2019). Dry film with the initial weight (W_d) was immersed in distilled water until it reached a swelling-equilibrium state at room temperature, followed by wiping off the surface water with filter paper to determine its wet weight (W_s). The measurement was repeated for three times. The *SR* was calculated according to the following equation:

$$SR(\%) = \frac{W_s - W_d}{W_d} \times 100\% \quad (2)$$

where W_s and W_d were the swollen and initial dry weight of the films, respectively.

Film thickness was measured using a micrometer (Lorentzen & Wettre, accuracy of 0.001 mm). The average value of five thickness measurements at different position per type of film was used in all calculations.

Tensile testing was performed on an Intron Universal Testing Machine 5566 based on the "ASTM D882-12" standard method. The films were cut into 10 mm×70 mm rectangular strips and tested with five repetitions for each film. The grips length was set at 30 mm, and the strain rate with 4 mm/min was used. The measurement was repeated for five times.

Water vapor permeability (WVP) of the films was characterized according to Kurek et al. (Kurek et al. 2018) with little modification. The films were sealed on a test vessel with a diameter of 28.0 cm containing 40 g dried silica gel. Then the bottles were placed in a desiccator containing water at 20 °C, and weighted periodically at intervals of 24 h for 7 days. WVP (g s^{-1} m^{-1} Pa^{-1}) was calculated from the change in the bottle weight versus time at the steady state using the following equation:

$$WVP = \frac{w \times L}{t \times A \times \Delta p} \quad (3)$$

where w is the weight gained (g); t is the elapsed time (s); A is the film area exposed to the moisture transfer (m^2); L is the film thickness (m); Δp is water vapor pressure difference between the two sides of the film (Pa). Three replicates for each film type were done.

Antibacterial activity of the films against *E. coli* and *S. aureus* was investigated using disc diffusion method (Zhang et al. 2019b). The films were cut into 15 mm pieces, and placed on *E. coli* and *S. aureus* cultured agar plates, and then incubated at 37 °C for 24 h. The antibacterial inhibition zone (W_{inh}) was calculated using the following equation:

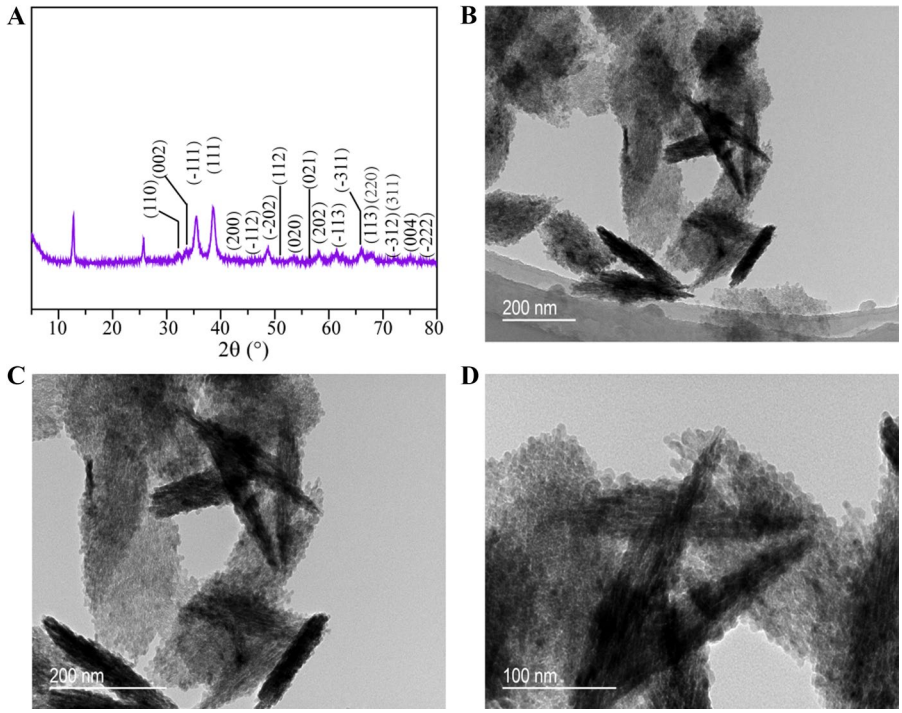

Fig. 1 XRD (**A**) spectrum and TEM (**B**, **C**, **D**) images of CuO nanoparticles

$$W_{inh} = \frac{d_1 - d_2}{2} \quad (4)$$

where d_1 is the total diameter of the inhibition zone and the film, and d_2 is the diameter of the film (15 mm). Three replicates for each film type were carried out.

The one-way analysis of variance (ANOVA) was used for multiple comparisons by SPSS 20.0 software package. Data were expressed as mean ± standard deviation. The level of $p \leq 0.05$ is used to evaluate the significant differences between two samples.

Results and discussion

Structure of synthesized CuO nanoparticles

Previous works have well studied the structural properties of CuO by the precipitation of copper ion precursor under aqueous alkaline environment (Booshehri et al. 2015; Cudennec and Lecerf 2003). Briefly, $Cu(OH)_2$ was firstly formed and then transformed to stable CuO through $Cu(OH)_4^{2-}$ intermediate species. In the XRD spectra of CuO nanoparticles (Fig. 1A), all observable peaks can be attributed to the diffraction of CuO with a monoclinic structure (DPF 01–080–1916). From TEM images (Fig. 1B–D), the CuO nanoparticles consist of self-assembled nanorods with diameters of around 50–100 nm.

Synthesis and structural characterization of the cross-linked CS nanocomposite films

The cross-linked CS nanocomposite films with versatile structural properties were effectively prepared by simultaneous cross-linking and in-situ loading (as shown in Scheme 1a). Specifically, ECH was chosen as the cross-linker, and CuO nanoparticles were in-situ loaded onto CS film matrix. The contents of HEC and ECH were controlled to tune the functional properties of the films to better match the application requirements. According to previous studies (Kurek et al. 2018; Zhao et al. 2016), the complex cross-linking reactions occurred between CS and HEC, and the schematic depiction of putative cross-linking reactions is shown in Scheme 1. The –NH groups from CS molecules can react with the –OH groups in HEC molecules to form cross-linked structure (as shown in Scheme 1b); the –NH and –OH groups on the CS molecules can form intermolecular cross-linked

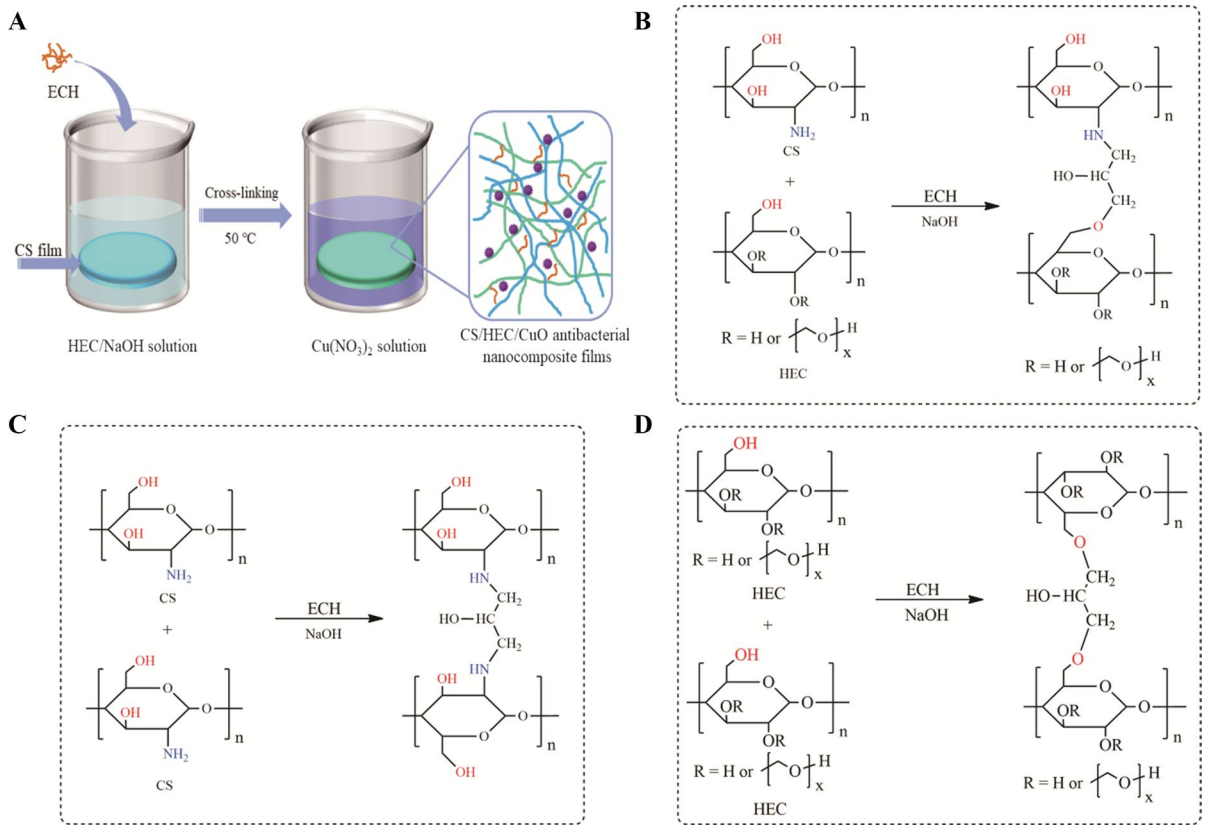

Scheme 1 Process for the fabrication of CS-based antibacterial nanocomposite films by simultaneous cross-linking with HEC and in-situ loading with CuO nanoparticles **a**; Putative cross-linking reactions of CS and HEC with ECH: reactions between CS and HEC **b**, CS and CS **c**, and HEC and HEC **d**, respectively

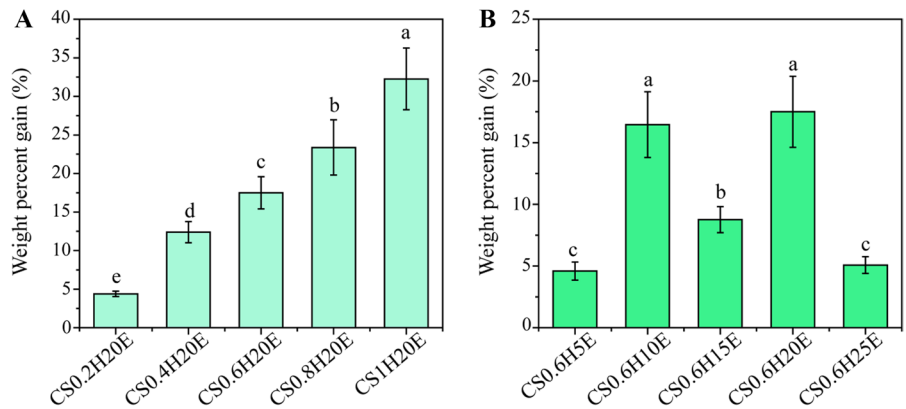

Fig. 2 HEC loading efficiency (*L*) of the cross-linked CS nanocomposite films

structure with other CS molecules (as shown in Scheme 1c); the –OH groups from HEC molecules can form intermolecular cross-linked structure with other HEC molecules (as shown in Scheme1d). Therefore, there is competition among the three potential reactions, making it complex to confirm the cross-linking degree. In order to prove the success of cross-linking reaction, the HEC loading efficiency (*L*) of the films was investigated. From Fig. 2A, increasing the HEC content from 0.2:1 to 1:1, the *L* of the films developed from 4.37 ± 0.35% to 32.26 ± 4.01%, indicating successful and intensified cross-linking

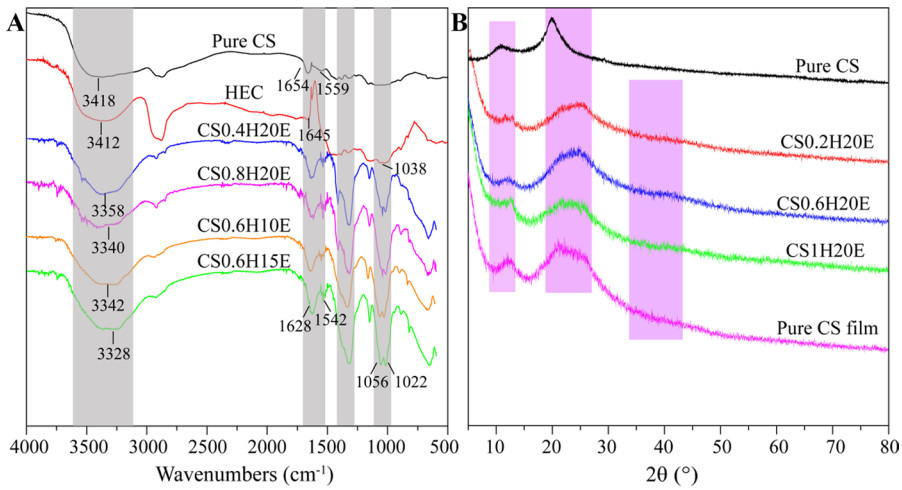

Fig. 3 FT-IR spectra (**A**) and XRD curves (**B**) of pure CS, HEC, and the cross-linked CS nanocomposite films

reaction occurred between CS and HEC. From Fig. 2B, comparatively, as ECH content increased from 5 to 10%, the *L* of the films developed, also indicating increased cross-linking reaction between CS and HEC. With further increase of ECH content to 15%, 20%, and 25%, the *L* of the films dramatically decreased firstly, and then increased to an optimum value before another decrease. This is probably due to the complex and competitive side-self-cross-linking between CS-CS and HEC-HEC.

To investigate the chemical reaction among each component of the composite film, FT-IR was applied to obtain the functional groups information of the films. As shown in Fig. 3A, the broad bands at 3200–3500 cm^{-1} are attributed to the O–H vibrations due to the hydroxyl groups of polysaccharide. For HEC, the symmetrical and asymmetrical C–H stretching is located at 2850–2980 cm^{-1}, and peaks at 1645 and 1038 cm^{-1} are ascribed to the absorbed water and C–O–C stretching vibration, respectively. For pure CS, two peaks at 1654 and 1559 cm^{-1} indicated the presence of amide I (C=O stretching) and amide II (N–H bending). In case of the cross-linked CS nanocomposite films, the –OH and –NH bands shifted to a lower area, indicating the cross-linking effect. Comparatively, with the increased HEC and ECH contents, this shifting of these bands became increasingly obvious, indicating intensified cross-linking reactions. In addition, the –NH bands of CS were apparently weakened, indicating that most of the –NH groups of CS have reacted with epoxy groups on the ECH and thus cross-linked with the –OH of HEC. Moreover, after the incorporation of HEC, the representative intense peak assigned to C–O stretching (ether bond C–O–C) was separated into two bands around 1056 and 1022 cm^{-1}.

Figure 3B shows the XRD patterns of the prepared samples. For the pure CS, two crystal forms existed: form I and form II depicted the major crystalline peaks at 10.9° and 20.1°, respectively. These two main peaks shifted to 12.4° and 23.2°, respectively, in the spectra of CS film loading with CuO, indicating that the incorporation of CuO particles disrupted the regular order of polymer chains. Similar results could be observed in CS/Ag/ZnO composite films (Li et al. 2010). After cross-linking with HEC, no palpable change in the main crystalline structure of CS was observed, probably due to the relative low content of HEC in the films. Furthermore, the characteristic peaks appear at around 35–40° after deposition process suggest the occurrence of CuO particles.

Morphology analyses

Physical appearance is the most intuitive property of the film materials. All the CuO loaded nanocomposite films showed aquamarine color (Fig. 4A). Comparatively, pure CS film showed relative higher transparency and brighter surface. After cross-linking with HEC, the transparency of the films reduced. Notably, the edges of pure CS film showed obvious folds and crimps, while the cross-linked CS nanocomposite films had relative smooth morphologies. This is probably due to the cross-linking reaction which could consume the –NH and –OH of CS, that is, decrease

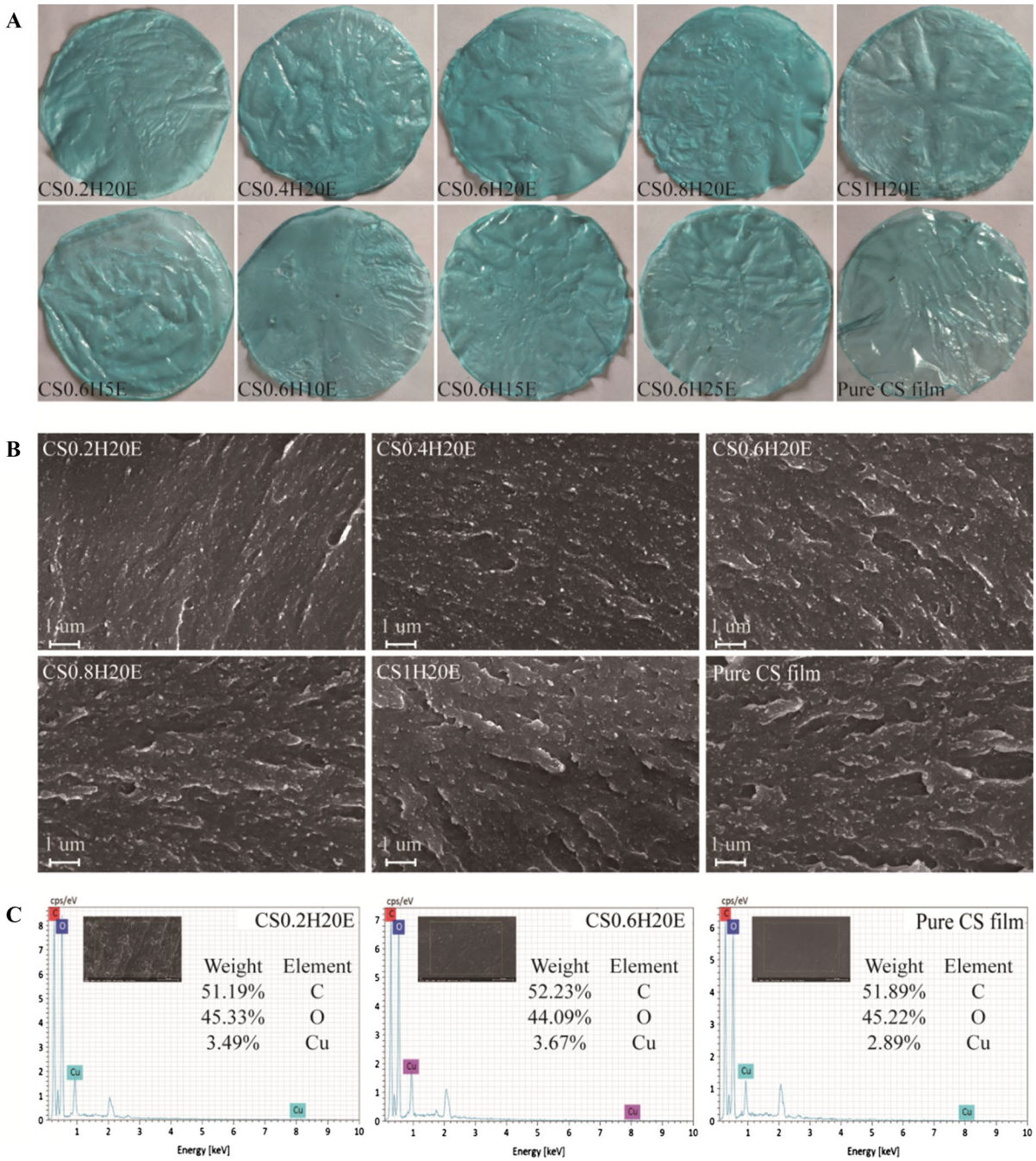

Fig. 4 Physical appearances (**A**), SEM images (**B**, cross section) and EDS spectra (**C**) of the cross-linked CS nanocomposite films

the hydrogen bonding interactions with water upon drying process.

SEM was used to characterize the cross-section morphology of the cross-linked CS nanocomposite films, as shown in Fig. 4B. The cross-section images of the samples displayed inconspicuous differences. Basically, the films were compact, dense, and uniform at cross-section, and no obvious voids were observed. This is probably due to the good compatibility among the cross-linked components, which may not affect

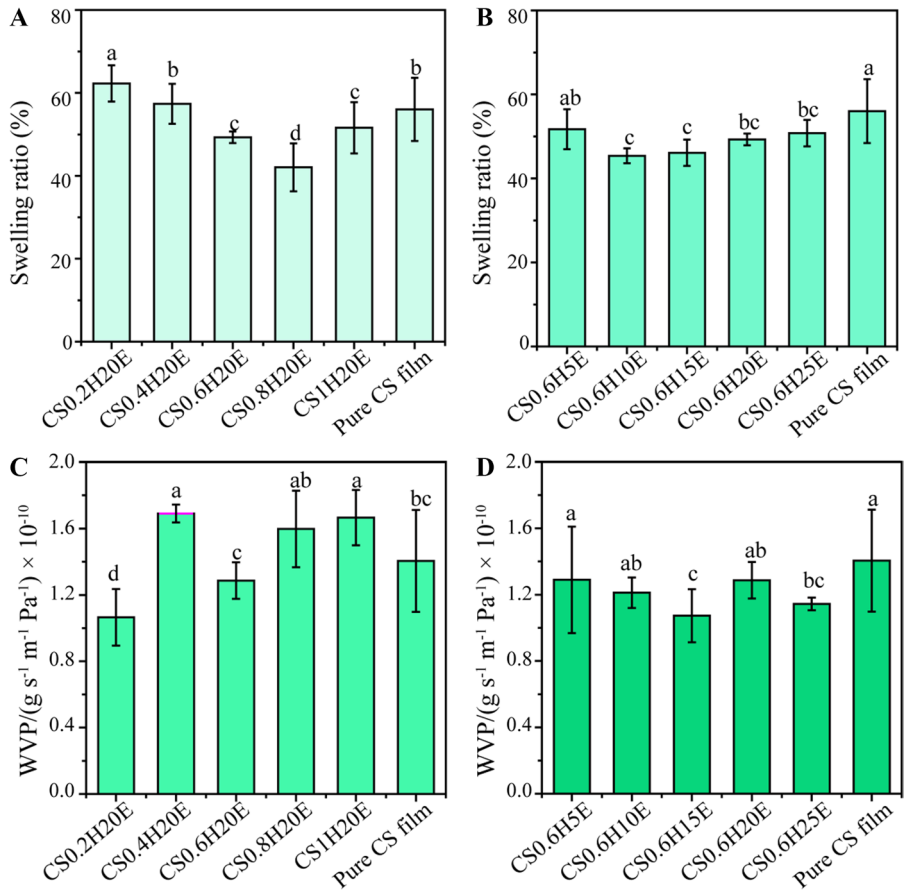

Fig. 5 Swelling ratio (**A**, **B**) and water vapor permeability (**C**, **D**) of the cross-linked CS nanocomposite films

the crystalline structure of CS matrix. This result is in accordance with the XRD analysis.

To analyze the elemental composition and determine the deposition of CuO onto CS film matrix, elemental mapping and EDS spectra were investigated. From Fig. 4C, Cu element was observed on the films, indicating the successful loading of CuO by in-situ depositing method. Besides, as compared with pure CS film, the relative weight contents of C and O elements increased with the increase amount of HEC, further indicating the increased cross-linking reaction between CS and HEC.

Swelling ratio and water vapor permeability

The *SR* values of both pure CS film and the cross-linked CS nanocomposite films were investigated, as shown in Fig. 5A. The pure CS film showed a relative high *SR* value, probably due to its interactions with water by the presence of free hydroxyl and amine groups. After adding 0.2:1 of HEC, the *SR* value of the films increased to 62.27 ± 4.38%, probably due to the inherent hydrophilicity of HEC. However, further increase of HEC content to 0.8:1 reduced the *SR* value to 42.05 ± 5.79%, probably due to the intensified cross-linking reaction between HEC and CS matrix. But excessive amount of HEC (1:1) resulted in an increase of *SR* value (51.58 ± 6.18%). From Fig. 5B, the results showed that the cross-linking of the films led to a decreased *SR* value. This is probably due to the consumption of CS hydrophilic hydroxyl and amine groups as they covalently bonded with cross-linking ECH and not available for interacting with water molecules, which resulted in a decrease of *SR* value (Priyadarshi et al. 2018). Similar results could also be observed in the other cross-linked CS films (Hafsa et al. 2016; Priyadarshi et al. 2018).

The water barrier ability of films is important for food packaging. In the case of dry food packaging, the moisture barrier ability is required to protect the

food from deterioration due to the moisture. On the other hand, the fresh product need to retain the moisture and avoid dehydration (Priyadarshi et al. 2018). The WVP of the cross-linked CS nanocomposite films is shown in Fig. 5C, D. The CuO nanoparticles reinforced pure CS film achieved $1.40 \pm 0.31 \times 10^{-10}$ g s^{-1} m^{-1} Pa^{-1} in WVP, which was lower than the value obtained in previous literatures (Bourbon et al. 2011; Costa et al. 2015). This is probably due that the resistibility of film against vapor permeation is closely related to the micro paths in the microstructure network. The WVP of the films generally increased with the increase of HEC content, which can be explained by the higher hydrophilicity and permeability of the films introduced by HEC. Based on the "adsorption-diffusion-desorption" mechanism (Yao et al. 2019), the incorporation of hydrophilic HEC improved the opportunity of adsorbing water molecules and thus increasing its WVP. The WVP decreased as the increase of ECH content. It can be explained based on the model of tortuosity (Vaezi et al. 2019). From FT-IR results, the cross-linking reaction between CS and HEC developed with higher content of ECH, which was beneficial for the formation of network structure, creating a tortuous pathway for water vapor molecules to permeate the film.

Mechanical properties

Mechanical properties of packaging films are essential to resist the stress appearing during the transport and storage processes. For pure CS film, there is a broad range of reported mechanical properties data in the literatures, mainly due to the various structures of CS (deacetylation degree and molecular weight) and preparation method (solvent, storage time and measurement conditions) (Cazón and Vázquez 2019). The CS-based nanocomposite films with ECH as the cross-linker have shown decent mechanical properties. In the present study, as shown in Fig. 6, the tensile strength of pure CS film was 55.95 ± 2.06 MPa. The tensile strength of the cross-linked CS nanocomposite films significantly increased ($p \leq 0.05$) with increasing the HEC content and reached a maximum value of 77.02 ± 3.26 MPa with HEC of 1:1. The tensile strength did not strongly correlated with the ECH

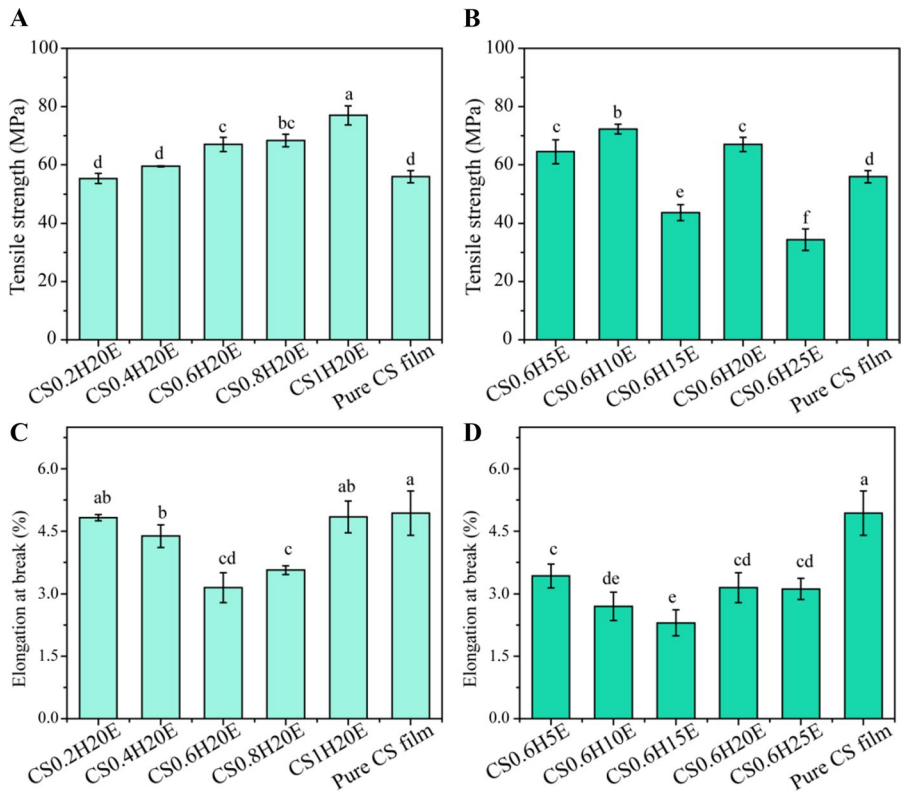

Fig. 6 Tensile strength (**A**, **B**) and elongation at break (**C**, **D**) of the cross-linked CS nanocomposite films obtained under different conditions

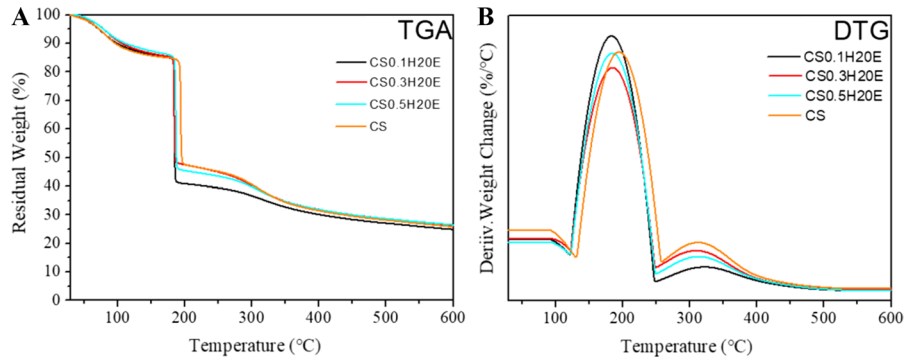

Fig. 7 TGA/DTG curves of CS and the cross-linked CS nanocomposite films

content, and a maximum value of 72.31 ± 1.65 MPa was achieved with 10% of ECH (Fig. 6B). As reported in previous literatures (Yao et al. 2019; Zhao et al. 2016), the complex cross-linking reactions occurred between CS and HEC using ECH as a cross-linker. The irregular tensile strength variation of the films with the increased ECH concentration is probably due to the complicated and competitive side-self-cross-linking between CS-CS and HEC-HEC.

From Fig. 6C, D, the elongation at break of the cross-linked CS nanocomposite films showed different trend. The elongation at break values significantly decreased ($p \leq 0.05$) with the increased HEC and ECH contents, indicating that the increased cross-linking reaction lowered the stretch-ability of the films.

Thermogravimetric analyses

TGA/DTG (Fig. 7) was applied to investigate the thermal stability of the films. The films exhibited two major stages of weight loss. From the TGA curves, the initial weight loss (about 15%) at around 100 °C is attributed to the evaporation of water. The second stage is corresponded to the organic matter loss and thermal degradation of CS (Lozano-Navarro et al.

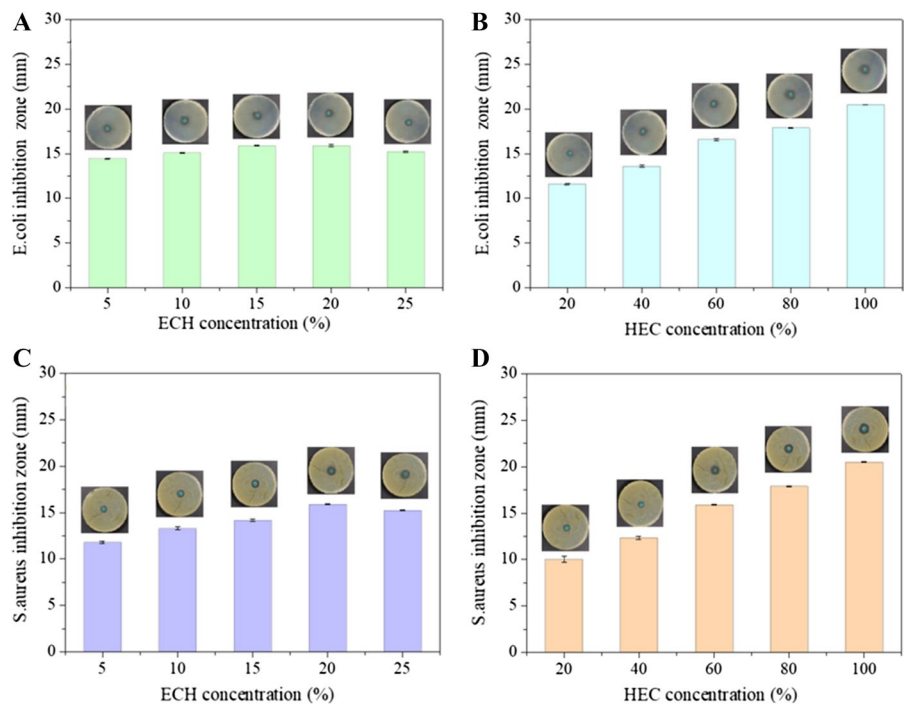

Fig. 8 Antimicrobial activities against E.coli (**A**, **B**) and S.aureus (**C**, **D**) of the cross-linked CS nanocomposite films obtained under different conditions

2018; Zhang et al. 2019b). The largest mass loss of CS mainly occurs between 180 and 320 °C, with a peak decomposition temperature at about 198 °C. Comparatively, the decomposition peak for the films is observed at about 185 °C, indicating the decreased thermal stability. This is probably due to the role of methylene groups in HEC molecules (Sen and Kahraman 2018), or the disruption of hydrogen bondings of CS after cross-linking reaction. From DTG curves, the cross-linked CS nanocomposite films and pure CS film showed the maximum decomposition peaks at about 183 °C and 198 °C, respectively, further indicating the decreased thermal stability of CS after cross-linking reaction. Additionally, the degradation peak at around 320 °C was probably attributed to the decomposition of the polysaccharide structure (Pereira et al. 2019). Similar results were reported by Santana et al. (Santana et al. 2017).

Antibacterial properties

Antibacterial activities of the cross-linked CS nanocomposite films against E.coli and S.aureus were evaluated by measuring the antibacterial inhibition zone, as shown in Fig. 8. In this study, the pure CS film showed better antibacterial ability against E.coli than S.aureus (not listed in Fig. 8). According to the previous study, the antibacterial mechanism of CS was attributed to the interaction between CS and cell membrane (Cazón et al. 2017). Therefore, different membranes, cell wall structure, cell physiology and metabolism of bacteria could result in different antibacterial activity of CS (Zhu et al. 2018).

Comparatively, the cross-linked CS nanocomposite films showed better antibacterial activities than pristine CS film. As shown in Fig. 8A–C, the antibacterial ability of the films against E.coli and S.aureus was slightly enhanced with the ECH content increased from 5% to 20%. While further increase of ECH content to 25% did not improve the antibacterial ability. This is probably due to the competitive side-self-cross-linking reaction. From Fig. 8B–D, the antibacterial ability of the films increased with higher HEC content, probably due to the developed cross-linking reaction with CS.

Conclusions

In this paper, the cross-linking of CS and HEC mediated by ECH and the in-situ loading of CuO nanoparticles were carried out in NaOH and $Cu(NO_3)_2$ solutions to prepare functional packaging films. The cross-linking reaction intensified with increased amount of HEC and ECH. Through consecutive in-situ coagulation, CuO nanoparticles were successfully deposited onto the film matrixes. The films exhibited compact, dense and uniform cross-section morphologies. Moreover, the novelty of our research showed that the cross-linked CS nanocomposite films exhibited decent mechanical properties and antibacterial ability, broadening its potential applications in active packaging area.

Acknowledgments This work supported by the National Natural Science Foundation of China (32001279), the Foundation and Applied Foundation Research Project of Guangdong Province (2019A1515110191), the Special Funds for Rural Rejuvenation Strategy of Guangdong Province (2020KJ265), the Fundamental Research Funds from the Guangzhou Livelihood Project (202002020080), the integration of key technologies in green production of olecranon peach (200830191605759), and the Guangdong key laboratory of Science and Technology of Lingnan Specialty Food (2021B1212040013).

Funding The authors have not disclosed any funding.

Declarations

Conflict of interest The authors declare no competing financial interest.

References

Almasi H, Mehryar L, Ghadertaj A (2019) Characterization of CuO-bacterial cellulose nanohybrids fabricated by in-situ and ex-situ impregnation methods. Carbohydr Polym 222:114995. https://doi.org/10.1016/j.carbpol.2019.114995

Arellano-Sandoval L, Delgado E, Camacho-Villegas TA, Bravo-Madrigal J, Manriquez-Gonzalez R, Lugo-Fabres PH, Toriz G, Garcia-Uriostegui L (2020) Development of thermosensitive hybrid hydrogels based on xylan-type hemicellulose from agave bagasse: characterization and antibacterial activity. MRS Commun 10:147–154. https://doi.org/10.1557/mrc.2019.165

Booshehri YA, Wang R, Xu R (2015) Simple method of deposition of CuO nanoparticles on a cellulose paper and its antibacterial activity. Chem Eng J 262:999–1008. https://doi.org/10.1016/j.cej.2014.09.096

Bourbon AI, Pinheiro AC, Cerqueire MA, Rocha CMR, Avides MC, Quintas MAC, Vicente AA (2011) Physico-chemical characterization of chitosan-based edible films incorporating bioactive compounds of different molecular weight. J Food Eng 106:111–118. https://doi.org/10.1016/j.jfoodeng.2011.03.024

Cao QQ, Zhang Y, Chen W, Meng XH, Liu BJ (2018) Hydrophobicity and physicochemical properties of agarose film as affected by chitosan addition. Int J Biol Macromol 106:1307–1313. https://doi.org/10.1016/j.ijbiomac.2017.08.134

Cao WL, Cheng MY, Ao Q, Gong YD, Zhao NM, Zhang XF (2012) Physical, mechanical and degradation properties, and Schwann cell affinity of cross-linked chitosan films. J Biomater Sci Polym Ed 16:791–807. https://doi.org/10.1163/1568562053992496

Cazón P, Vázquez M (2019) Mechanical and barrier properties of chitosan combined with other components as food packaging film. Environ Chem Lett 18:257–267. https://doi.org/10.1007/s10311-019-00936-3

Cazón P, Velazquez G, Ramirez JA, Vazquez M (2017) Polysaccharide-based films and coatings for food packaging: a review. Food Hydrocoll 68:136–148. https://doi.org/10.1016/j.foodhyd.2016.09.009

Čech Barabaszová K, Holešová S, Bílý M, Hundáková M (2020) CuO and CuO/vermiculite based nanoparticles in antibacterial PVAc nanocomposites. J Inorg Organomet Polym Mater 30:4218–4227. https://doi.org/10.1007/s10904-020-01573-y

Costa MJ, Cerqueira MA, Ruiz HA, Fougnies C, Richel A, Vicente AA, Teixeira JA, Aguedo M (2015) Use of wheat bran arabinoxylans in chitosan-based films: Effect on physicochemical properties. Ind Crop Prod 66:305–311. https://doi.org/10.1016/j.indcrop.2015.01.003

Cudennec Y, Lecerf A (2003) The transformation of Cu(OH)2 into CuO, revisited. Solid State Sci 5:1471–1474. https://doi.org/10.1016/j.solidstatesciences.2003.09.009

Ebrahimi Y, Peighambardoust SJ, Peighambardoust SH, Karkaj SZ (2019) Development of antibacterial carboxymethyl cellulose-based nanobiocomposite films containing various metallic nanoparticles for food packaging applications. J Food Sci 84:2537–2548. https://doi.org/10.1111/1750-3841.14744

Fu FY, Li LY, Liu LJ, Cai J, Zhang YP, Zhou JP, Zhang LN (2015) Construction of cellulose based ZnO nanocomposite films with antibacterial properties through one-step coagulation. ACS Appl Mater Interfaces 7:2597–2606. https://doi.org/10.1021/am507639b

Guan Y, Qi XM, Chen GG, Peng F, Sun RC (2016) Facile approach to prepare drug-loading film from hemicelluloses and chitosan. Carbohydr Polym 153:542–548. https://doi.org/10.1016/j.carbpol.2016.08.008

Guo JN, Xu QM, Zheng ZQ, Zhou SB, Mao HL, Wang B, Yan F (2015) Intrinsically antibacterial poly(ionic liquid) membranes: the synergistic effect of anions. ACS Macro Lett 4:1094–1098. https://doi.org/10.1021/acsmacrolett.5b00609

Hafsa J, Smach MA, Ben Khedher MR, Charfeddine B, Limem K, Majdoub H, Rouatbi S (2016) Physical, antioxidant and antimicrobial properties of chitosan films containing Eucalyptus globulus essential oil. LWT-Food Sci Technol 68:356–364. https://doi.org/10.1016/j.lwt.2015.12.050

Joubert F, Yeo RP, Sharples GJ, Musa OM, Hodgson DRW, Cameron NR (2015) Preparation of an antibacterial poly(ionic liquid) graft copolymer of hydroxyethyl cellulose. Biomacromolecules 16:3970–3979. https://doi.org/10.1021/acs.biomac.5b01300

Kumar S, Krishnakumar B, Sobral AJFN, Koh J (2019) Bio-based (chitosan/PVA/ZnO) nanocomposites film: thermally stable and photoluminescence material for removal of organic dye. Carbohydr Polym 205:559–564. https://doi.org/10.1016/j.carbpol.2018.10.108

Kurek M, Garofulić IE, Bakić MT, Ščetar M, Uzelac VD, Galić K (2018) Development and evaluation of a novel antioxidant and pH indicator film based on chitosan and food waste sources of antioxidants. Food Hydrocoll 84:238–246. https://doi.org/10.1016/j.foodhyd.2018.05.050

Li LH, Deng JC, Deng HR, Liu ZL, Li XL (2010) Preparation, characterization and antimicrobial activities of chitosan/Ag/ZnO blend films. Chem Eng J 160:378–382. https://doi.org/10.1016/j.cej.2010.03.051

Lozano-Navarro JI, Diaz-Zavala NP, Velasco-Santos C, Melo-Banda JA, Paramo-Garcia U, Paraguay-Delgado F, Garcia-Alamilla R, Martinez-Hernandez AL, Zapien-Castillo S (2018) Chitosan-starch films with natural extracts: physical chemical, morphological and thermal properties. Materials 11:120. https://doi.org/10.3390/ma11010120

Min TT, Zhu Z, Sun XL, Yuan ZP, Zha JW, Wen YQ (2020) Highly efficient antifogging and antibacterial food packaging film fabricated by novel quaternary ammonium chitosan composite. Food Chem 308:125682. https://doi.org/10.1016/j.foodchem.2019.125682

Peighambardoust SH, Beigmohammadi F, Peighambardoust SJ (2016) Application of organoclay nanoparticle in low-density polyethylene films for packaging of UF cheese. Packag Technol Sci 29:355–363. https://doi.org/10.1002/pts.2212

Pereira LA, Reis LDS, Batista FA, Mendes AN, Osajima JA, Silva EC (2019) Biological properties of chitosan derivatives associated with the ceftazidime drug. Carbohydr Polym 222:115002. https://doi.org/10.1016/j.carbpol.2019.115002

Priyadarshi R, Sauraj KBSH, Negi YS (2018) Chitosan film incorporated with citric acid and glycerol as an active packaging material for extension of green chilli shelf life. Carbohydr Polym 195:329–338. https://doi.org/10.1016/j.carbpol.2018.04.089

Raghavendra GM, Jung J, Kim D, Seo J (2017) Chitosan-mediated synthesis of flowery-CuO, and its antibacterial and catalytic properties. Carbohydr Polym 172:78–84. https://doi.org/10.1016/j.carbpol.2017.04.070

Santana ACSGV, Sobrinho JS, da Silva EC, Nunes LCC (2017) Preparation and physicochemical characterization of binary composites palygorskite–chitosan for drug delivery. J Therm Anal Calorim 128:1327–1334. https://doi.org/10.1007/s10973-016-6075-5

Sen F, Kahraman MV (2018) Preparation and characterization of hybrid cationic hydroxyethyl cellulose/sodium alginate polyelectrolyte antimicrobial films. Polym Advan Technol 29:1895–1901. https://doi.org/10.1002/pat.4298

Siripatrawan U, Kaewklin P (2018) Fabrication and characterization of chitosan-titanium dioxide nanocomposite film as ethylene scavenging and antimicrobial active food packaging. Food Hydrocoll 84:125–134. https://doi.org/10.1016/j.foodhyd.2018.04.049

Vaezi K, Asadpour G, Sharifi H (2019) Effect of ZnO nanoparticles on the mechanical, barrier and optical properties of thermoplastic cationic starch/montmorillonite biodegradable films. Int J Biol Macromol 124:519–529. https://doi.org/10.1016/j.ijbiomac.2018.11.142

Verlee A, Mincke S, Stevens CV (2017) Recent developments in antibacterial and antifungal chitosan and its derivatives. Carbohydr Polym 164:268–283. https://doi.org/10.1016/j.carbpol.2017.02.001

Wang B, Sui J, Yu B, Yuan C, Guo L, Abd El-Aty AM, Cui B (2021) Physicochemical properties and antibacterial activity of corn starch-based films incorporated with Zanthoxylum bungeanum essential oil. Carbohydr Polym 254:117314. https://doi.org/10.1016/j.carbpol.2020.117314

Wang XH, Wang SY, Liu W, Wang S, Zhang LG, Shang RR, Hou QX, Li JS (2019) Facile fabrication of cellulose composite films with excellent UV resistance and antibacterial activity. Carbohydr Polym 225:115213. https://doi.org/10.1016/j.carbpol.2019.115213

Xie YY, Hu XH, Zhang YW, Wahid F, Chu LQ, Jia SR, Zhong C (2020) Development and antibacterial activities of bacterial cellulose/graphene oxide-CuO nanocomposite films. Carbohydr Polym 229:115456. https://doi.org/10.1016/j.carbpol.2019.115456

Yao YJ, Wang HR, Wang RR, Chai Y (2019) Novel cellulose-gelatin composite films made from self-dispersed microgels: structure and properties. Int J Biol Macromol 123:991–1001. https://doi.org/10.1016/j.ijbiomac.2018.11.184

Yeng CM, Husseinsyah S, Ting SS (2015) A comparative study of different crosslinking agent-modified/corn cob biocomposite films. Polym Bull 72:791–808. https://doi.org/10.1007/s00289-015-1305-8

Yousefi P, Hamedi S, Garmaroody ER, Koosha M (2020) Antibacterial nanobiocomposite based on halloysite nanotubes and extracted xylan from bagasse pith. Int J Biol Macromol 160:276–287. https://doi.org/10.1016/j.ijbiomac.2020.05.209

Yu Z, Li BQ, Chu JY, Zhang PF (2018) Silica in situ enhanced PVA/chitosan biodegradable films for food packages. Carbohydr Polym 184:214–220. https://doi.org/10.1016/j.carbpol.2017.12.043

Yuan TZ, Zeng JS, Wang B, Cheng Z, Gao WH, Xu J, Chen KF (2020) Silver nanoparticles immobilized on cellulose nanofibrils for starch-based nanocomposites with high antibacterial, biocompatible, and mechanical properties. Cellulose 28:855–869. https://doi.org/10.1007/s10570-020-03567-y

Zhang H, Liu PW, Peng XW, Chen SL, Zhang K (2019a) Interfacial synthesis of cellulose-derived solvent-responsive nanoparticles via schiff base reaction. ACS Sustain Chem Eng 7:16595–16603. https://doi.org/10.1021/acssuschemeng.9b03919

Zhang X, Liu YP, Yong HM, Qin YS, Liu J, Liu J (2019b) Development of multifunctional food packaging films based on chitosan, TiO2 nanoparticles and anthocyanin-rich black plum peel extract. Food Hydrocolloid 94:80–92. https://doi.org/10.1016/j.foodhyd.2019.03.009

Zhang XQ, Luo WH, Xiao NY, Chen MJ, Liu CF (2020) Construction of functional composite films originating from hemicellulose reinforced with poly(vinyl alcohol) and nano-ZnO. Cellulose 27:1341–1355. https://doi.org/10.1007/s10570-019-02878-z

Zhao YT, He M, Zhao L, Wang SQ, Li YP, Gan L, Li MM, Xu L, Chang PR, Anderson DP, Chen Y (2016) Epichlorohydrin-cross-linked hydroxyethyl cellulose/soy protein isolate composite films as biocompatible and viodegradable implants for tissue engineering. ACS Appl Mater Interfaces 8:2781–2795. https://doi.org/10.1021/acsami.5b11152

Zhu Z, Cai H, Sun DW (2018) Titanium dioxide (TiO_2) photocatalysis technology for nonthermal inactivation of microorganism in foods. Trends Food Sci Tech 75:23–25. https://doi.org/10.1016/j.tifs.2018.02.018